Intraprotein transfer of the quinone analogue inhibitor 2,5-dibromo-3-methyl-6-isopropyl-*p*-benzoquinone in the cytochrome b_6f complex

Jiusheng Yan, Genji Kurisu*, and William A. Cramer†

Department of Biological Sciences, Purdue University, West Lafayette, IN 47907

Edited by Pierre A. Joliot, Institut de Biologie Physico-Chimique, Paris, France, and approved November 10, 2005 (received for review June 13, 2005)

Details are presented of the structural analysis of the cytochrome b_6f complex from the thermophilic cyanobacterium, *Mastigocladus laminosus*, in the presence of the electrochemically positive (*p*)-side quinone analogue inhibitor, 2,5-dibromo-3-methyl-6-isopropyl-benzoquinone (DBMIB). One DBMIB binding site was found. This site is peripheral to the quinone binding space defined by the binding sites of other *p*-side inhibitors previously resolved in cytochrome bc_1/b_6f complexes. This high-affinity site resides in a *p*-side interfacial niche bounded by cytochrome *f*, subunit IV, and cytochrome b_6, is close (8 Å) to the *p*-side heme *b*, but distant (19 Å) from the [2Fe-2S] cluster. No significant electron density associated with the DBMIB was found elsewhere in the structure. However, the site at which DBMIB can inhibit light-induced redox turnover is within a few Å of the [2Fe-2S] cluster, as shown by the absence of inhibition in mutants of *Synechococcus* sp. PCC 7002 at iron sulfur protein-Leu-111 near the cluster. The ability of a minimum amount of initially oxidized DBMIB to inhibit turnover of WT complex after a second light flash implies that there is a light-activated movement of DBMIB from the distal peripheral site to an inhibitory site proximal to the [2Fe-2S] cluster. Together with the necessary passage of quinone/quinol through the small Q_p portal in the complex, it is seen that transmembrane traffic of quinone-like molecules through the core of cytochrome *bc* complexes can be labyrinthine.

photosynthetic membrane proteins | energy transduction | transmembrane traffic

The cytochrome b_6f complex together with the two reaction center complexes of oxygenic photosynthesis sustain electron transfer and generation of a proton electrochemical potential gradient across thylakoid membranes (1). As in the cytochrome bc_1 complex of mitochondria and purple photosynthetic bacteria, the transmembrane proton transfer functions of the b_6f complex are accomplished by oxidization and reduction of lipophilic quinol and quinone, respectively, on the *p*- (electrochemically positive) and *n*- (electrochemically negative) sides of the complex (Fig. 1*A*). X-ray structures of the dimeric b_6f complex have been obtained from the thermophilic cyanobacterium *Mastigocladus laminosus* (2) in the native state (3.4 Å), in the presence of the *p*-side quinone analogue inhibitor tridecyl-stigmatellin (TDS) [3.0 Å; Protein Data Bank (PDB) ID code 1VF5] or 2,5-dibromo-3-methyl-6-isopropyl-*p*-benzoquinone (DBMIB) (3.8 Å; PDB ID code 2D2C), and from the green alga, *Chlamydomonas reinhardtii*, cocrystallized with TDS (3.1 Å; PDB ID code 1Q90) (3). These structures define binding sites of quinol analogue inhibitors that could be compared with data on the binding sites of *p*-side inhibitors obtained from x-ray structure analysis of the mitochondrial bc_1 complex (4–11).

The cytochrome b_6f complex is a 220-kDa homodimeric complex composed of eight subunits with 13 transmembrane helices per monomer, two *p*-side extra-membrane soluble domains, and seven prosthetic groups (Fig. 1*A*). The cytochrome b_6 subunit contains four transmembrane helices, two *b*-type hemes (b_p and b_n), located near the *n*- and *p*-sides of the membrane, and a unique covalently bound "heme *x*" (2), also called c_i (3). Subunit IV, with three transmembrane helices, participates in the binding of the single chlorophyll *a* and β-carotene molecule present in each monomer and in the binding of plastoquinone (PQ). Cytochrome b_6 and subunit IV form the core of the dimeric complex. The 3D structure of cytochrome b_6 is almost identical to that of the N-terminal half of the cytochrome *b* subunit in the bc_1 complex, and subunit IV is similar to the C-terminal half of the cytochrome *b*, as predicted by homology of sequences and hydropathy plots (12). Four small hydrophobic subunits (molecular mass = 3.3–4.3 kDa), Pet-G, Pet-L, Pet-M, and Pet-N, each having a single transmembrane helix, form a peripheral "picket fence" around the core. The cytochrome *f* and iron-sulfur protein (ISP) subunits form a large extra-membrane *p*-side soluble domain that contains a *c*-type heme and [2Fe-2S] cluster and are embedded in the membrane by a single C- or N-terminal transmembrane helix, respectively. These two subunits are functionally analogous to cytochrome c_1 and the ISP subunit in the cytochrome bc_1 complex (13–15).

The proton-motive pathway of the linear electron transfer through the b_6f complex (Fig. 1*A*) is believed to be similar in many aspects to that catalyzed by the bc_1 complex (14–20). Plastoquinol is oxidized in a bifurcated manner at the Q_p site of the b_6f complex. One electron is transferred to the high potential electron transfer chain that consists of the [2Fe-2S] cluster and cytochrome *f*. Two protons are thereby discharged into the *p*-side water phase, and the other electron is forced to flow through the low-potential components (hemes b_p, b_n, and presumably heme *x*) to reduce PQ on the *n*-side of the membrane.

Crystallographic analysis of the bc_1 and b_6f complexes has defined a large *p*-side quinone-binding (Q_p) space (2–11), in which most of the reactive head groups of these inhibitors reside in a pocket (Q_p) and the tails, if present, extend into a narrow portal connecting the pocket to the large intermonomer quinone-exchange cavity. The Q_p space is portrayed in Fig. 6, which is published as supporting information on the PNAS web site. The Q_p site quinol analogue inhibitors block binding of the physiological quinol at the Q_p site and thereby inhibit *p*-side charge transfer, with the exception that the "ring-out" binding mode of TDS inhibits inefficiently (21). The Q_p pocket lies between heme b_p and the [2Fe-2S] cluster and is surrounded by the tilted *p*-side half of the C- transmembrane helix, the N-

Conflict of interest statement: No conflicts declared.

This paper was submitted directly (Track II) to the PNAS office.

Abbreviations: DBMIB, 2,5-dibromo-3-methyl-6-isopropyl-*p*-benzoquinone; ISP, iron-sulfur protein; *n*-, electrochemically negative; *p*-, electrochemically positive; PQ, plastoquinone; TDS, tridecyl-stigmatellin.

Data deposition: The atomic coordinates have been deposited in the Protein Data Bank, www.pdb.org (PDB ID code 2D2C).

*Present address: Department of Life Sciences, Graduate School of Arts and Sciences, University of Tokyo, Komaba 3-8-1, Meguro, Tokyo 153-8902, Japan.

†To whom correspondence should be addressed. E-mail: waclab@purdue.edu.

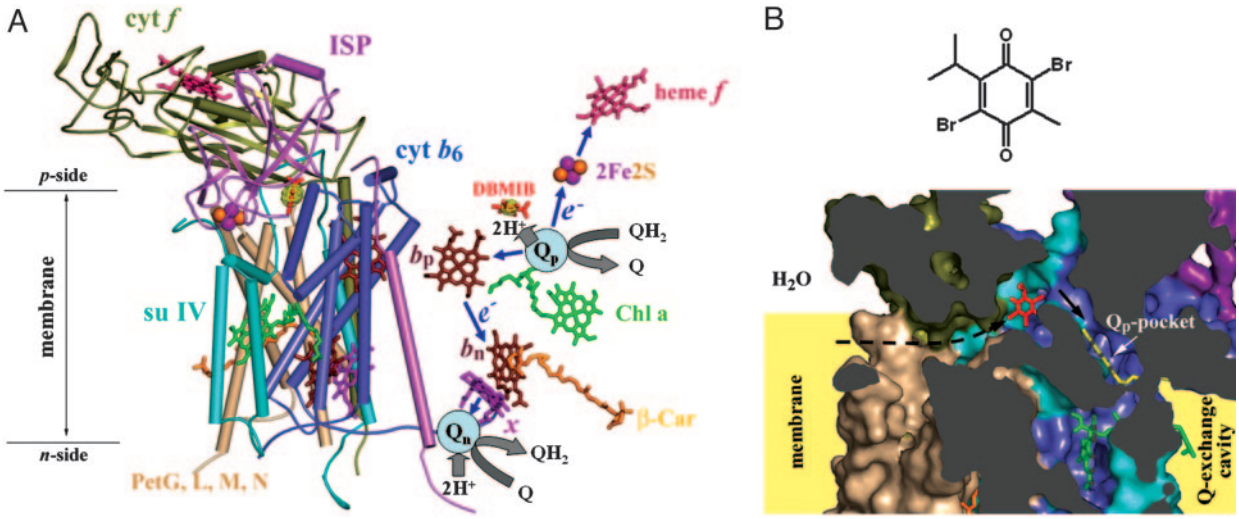

Fig. 1. Structure model of the cytochrome b_6f complex with bound DBMIB. (*A*) Model (3.8 Å) of the dimeric b_6f complex from *M. laminosus* with bound DBMIB. To emphasize the prosthetic groups and electron transfer pathways, (*Left*) all polypeptide components are shown in one monomer with α-helices viewed as cylinders, whereas (*Right*) only DBMIB and the prosthetic groups are shown in the other monomer. The electron density of DBMIB is shown in yellow with a contour level of 6 σ. The electron transfer pathways (see text for details) in one monomer (*Right*) are shown schematically. 2Fe2S, iron-sulfur cluster; blue arrows, electron transfer paths; b_p, heme b_p; b_n, heme b_n; β-Car, β-carotene; Chl *a*, chlorophyll *a*; e^-, electron; H^+, proton; Q, quinone; QH_2, quinol; Q_n, *n*-side quinone binding site (reduction site); Q_p, *p*-side quinone binding site (oxidation site); *x*, heme *x*. For clarity, endogenous PQ molecules bound at the Q_n site are not shown. (*B*) (*Upper*) Chemical structure of DBMIB and (*Lower*) cross-sectional view of its binding site and position relative to the Q_p pocket. To show the position of the Q_p pocket, a ring-in TDS molecule (yellow) from the *C. reinhardtii* structure is superimposed on the structure. The black arrows indicate the putative pathway for the entry of DBMIB to the Q_p pocket from the membrane lipid phase. Color code is the same as in *A*. All protein structural figures were drawn with PYMOL (http://pymol.sourceforge.net).

terminal half of the *cd*1 helix of cytochrome b_6, and the C-terminal end of the *ef* loop of subunit IV including the Pro-Glu-Trp-Tyr (PEWY) motif and the small *ef* helix.

DBMIB is an effective *p*-side inhibitor of the b_6f complex (22). As with other quinone analogue inhibitors, DBMIB is expected to inhibit electron transfer by displacing plastoquinol binding at the Q_p site (23–26). However, x-ray crystallographic analysis at a resolution of 3.8 Å of the b_6f complex from *M. laminosus*, cocrystallized with DBMIB, indicated that this inhibitor is bound in a peripheral site that is outside the Q_p pocket and far (19 Å) from the ISP [2Fe-2S] cluster. In the present study, we present structure data for the b_6f–DBMIB complex and investigate whether a DBMIB molecule bound at the peripheral site can function as an effective inhibitor at the [2Fe-2S] cluster.

Materials and Methods

Crystallographic Analysis. Crystallization and structure determination of the *M. laminosus* b_6f complex was carried out as described (2, 27). For cocrystallization, DBMIB was added at a concentration (0.5 mM) five times that of cytochrome *f* in the complex, and the insoluble fraction of DBMIB was removed by centrifugation. Two crystal structures at 3.4- and 3.8-Å resolution were originally obtained (2), which were derived from data collected by an image plate and charge-coupled device-based detector, respectively. The bound DBMIB molecule was found in the same position in both crystals, and we considered that the two structures contained similar information. However, it was subsequently found that the 3.8-Å structure suffered less radiation damage, presumably because of a shorter time taken for data collection. Thus, the 3.8-Å data have slightly better crystallographic statistics compared with those obtained at 3.4 Å and are used in the present study. The refinement statistics are summarized in Table 1.

Construction of Mutant Strains and Growth of Cultures. Mutant strains, WT^S, ISP-L111A, and ISP-L111Y, of *Synechococcus* sp. PCC 7002 were constructed and grown in medium A (28) as described (21, 29).

Flash Kinetic Spectroscopy. Flash-induced oxidation and rereduction of cytochrome f/c_6 in intact cells of *Synechococcus* sp. PCC 7002, resuspended at 5 μM chlorophyll in 50 mM Hepes (pH 7.5), 0.1 M NaCl, 10 mM $NaHCO_3$, 10 μM 3-(3′,4′-dichlorophenyl)-1,1-dimethylurea, 10 μM carbonyl cyanide *p*-trifluoromethoxy-phenylhydrazone, and 1 mM KCN, were monitored in the α-band absorbance region ($\Delta A_{556-540nm}$), using a laboratory-built single-beam spectrometer with an Xe flash actinic source, as described (21, 29, 30). Flash-induced redox changes in cytochrome *f* in spinach thylakoids were measured under conditions as described in ref. 31 or the figure legends.

EPR Spectroscopy. EPR spectroscopy was performed with a Bruker (Billerica, MA) ESP300 E spectrometer operating at

Table 1. Refinement statistics

X-ray source	APS-19ID
Wavelength, Å	1.0
Cell constants, $P6_1$	
a, *b*, Å	156.6
c Å	361.8
Resolution range, Å	25–3.8
Completeness, %	93.1 (79.2)
R_{cryst}	0.276
R_{free}	0.378
RMSD bonds, Å	0.012
RMSD angles, °	1.9
Mean *B* values, Å^2	92.6

Values in parentheses apply to the highest-resolution shell. R_{cryst} and R_{free} were calculated from the working and test reflection sets, respectively; the test set comprised 3% of the total reflections not used in refinement. RMSD, rms deviation.

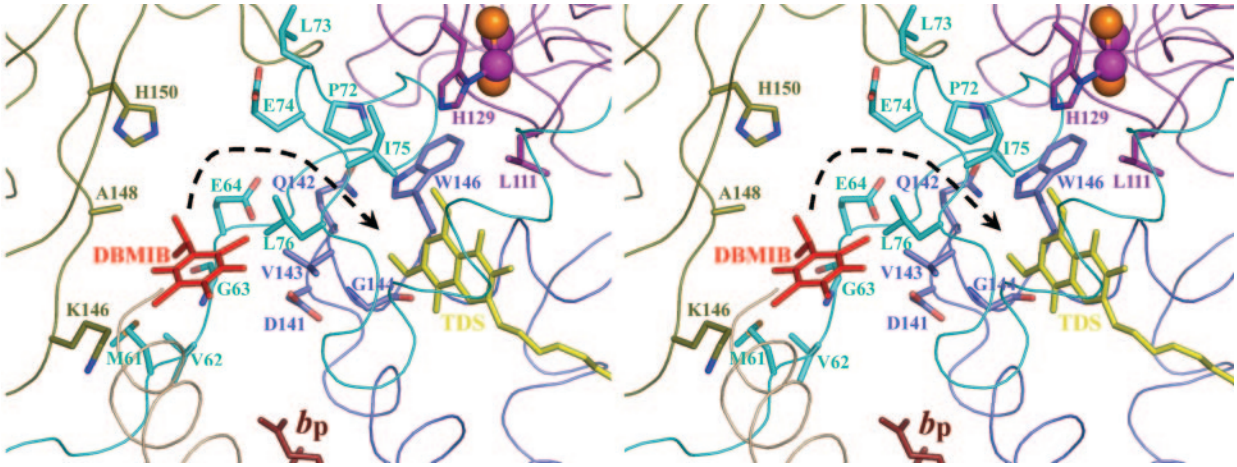

Fig. 2. Ribbon diagram (stereoview) of the peripheral DBMIB binding environment and its position relative to the [2Fe-2S] cluster and heme b_p. As in Fig. 1*B*, a ring-in TDS molecule (yellow) from *C. reinhardtii* structure is superimposed on the structure. Residues around the peripheral DBMIB binding site or located between the DBMIB binding niche and the Q_p pocket are shown as sticks (see text for details). Color code is the same as in Fig. 1. The black arrow shows the putative pathway for the movement of DBMIB to the Q_p pocket.

X-band. Instrument parameters were: microwave frequency, 9.4 GHz; temperature, 20 K; microwave power, 5 mW; modulation amplitude, 12.8 G; modulation frequency, 100 kHz; conversion time, 82 ms; time constant, 328 ms; and receiver gain, 1×10^5. Suspensions of the isolated *M. laminosus* cytochrome b_6f complex (10 μM) were prepared in 70 mM Tris·HCl (pH 7.5), 50 mM NaCl, 50 mM $MgCl_2$, 1 mM EDTA, 0.05% β-D-undecyl-maltoside, and 0.1 g/liter dioleolyl-phosphatidylcholine.

Results

Properties of the DBMIB Binding Sites. The overall structure of the *M. laminosus* b_6f complex cocrystallized with oxidized DBMIB at 3.8-Å resolution is indistinguishable from the structures of the native and TDS–b_6f complex at 3.4 and 3.0 Å. In the difference-Fourier map calculated with the $|F_{DBMIB}| - |F_{Native}|$ coefficient derived from DBMIB–b_6f minus native data and phases from multiple isomorphous replacement, the DBMIB molecule in the *M. laminosus* b_6f complex (Fig. 1*A*) was identified as a circular electron density 5 Å in diameter at contour level of 3 σ and 3.5 Å at 6-σ cut-off. However, this DBMIB binding site is located at an unexpected peripheral site, which is outside the Q_p pocket defined by the existing set of Q_p-analogue inhibitors (Fig. 6 and Fig. 7, which is published as supporting information on the PNAS web site) and 19 Å from the ISP [2Fe-2S] cluster. In contrast, no such significant electron density (>3 σ) was detected near the [2Fe-2S] cluster where DBMIB is expected to bind and exert its inhibitory effect on photosynthetic electron transport (23–26). This peripheral DBMIB binding site is in a *p*-side water/membrane interfacial niche, which is accessible from both water and membrane lipid phases (Fig. 1*B*) and bounded by cytochrome *f* and the subunit IV *ef* loop (Fig. 2). This DBMIB binding site is surrounded by residues 61–64 (Met-Val-Gly-Glu) and Leu-76 of the *ef* loop in subunit IV, Asp-141 and Val-143 at the N-terminal end of the *cd*1 helix in cytochrome b_6, and residues Lys-146, Ala-148, and His-150 of cytochrome *f* (Fig. 2). The position of the [2Fe-2S] cluster in the *M. laminosus* structures is shifted outward in the *p*-side direction by ~4 Å compared with that in the TDS-*C. reinhardtti* structure. Because the ISP is not involved in crystal contacts, the lack of interaction between ISP and DBMIB in the crystal structure is unlikely to be a crystallization artifact.

As inferred from EPR studies of the [2Fe-2S] cluster in spinach b_6f complex, there are two DBMIB binding sites within the complex: one high-affinity site that can be occupied by a stoichiometric amount of DBMIB and exerts a small effect on the EPR signal and one weak site at which excess DBMIB can bind and cause a major shift (from 1.89 to 1.94) of the g_y EPR signal (26, 32). A similar result was obtained in the present studies in which addition of one oxidized DBMIB per monomer of *M. laminosus* b_6f had little effect on the amplitude or position of the g_y = 1.90 or shifted 1.94 EPR signals (Fig. 3). However, higher concentrations of DBMIB (>2 molecules per monomer), which allow binding to a lower-affinity site close to the [2Fe-2S] cluster, did perturb the signal. An additional feature of these spectra is the appearance of a g = 1.97 signal that was not seen in spectra of the spinach complex. Therefore, consistent with the EPR results, the observed peripheral binding site in the *M. laminosus* structure must be a "high-affinity site" for oxidized DBMIB as it is the only site seen in the structure and located distal from the iron-sulfur cluster. Because of the requirement of a high concentration of the b_6f complex during crystallization and the limited solubility of DBMIB in water, a high ratio of DBMIB/b_6f and thereby a detectable DBMIB binding near the iron-sulfur cluster was not found in the crystal structure.

Effect of DBMIB on Flash-Induced Turnover of the b_6f Complex. The inhibitory effect of DBMIB on the electron transfer activity of the

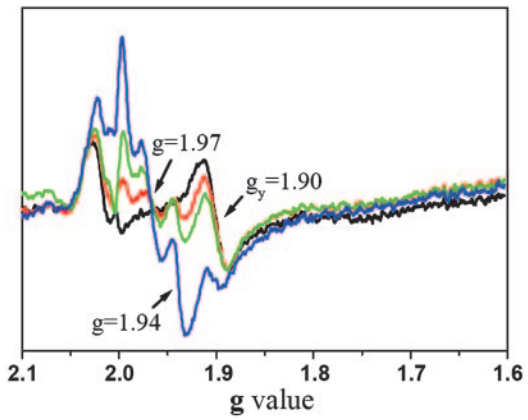

Fig. 3. Dependence of EPR spectrum from Rieske [2Fe-2S] in *M. laminosus* b_6f complex on DBMIB concentration. Spectra were measured in the absence (black) or the presence of one (red), two (green), or five (blue) molecules of DBMIB per monomer. See *Materials and Methods* for experimental details.

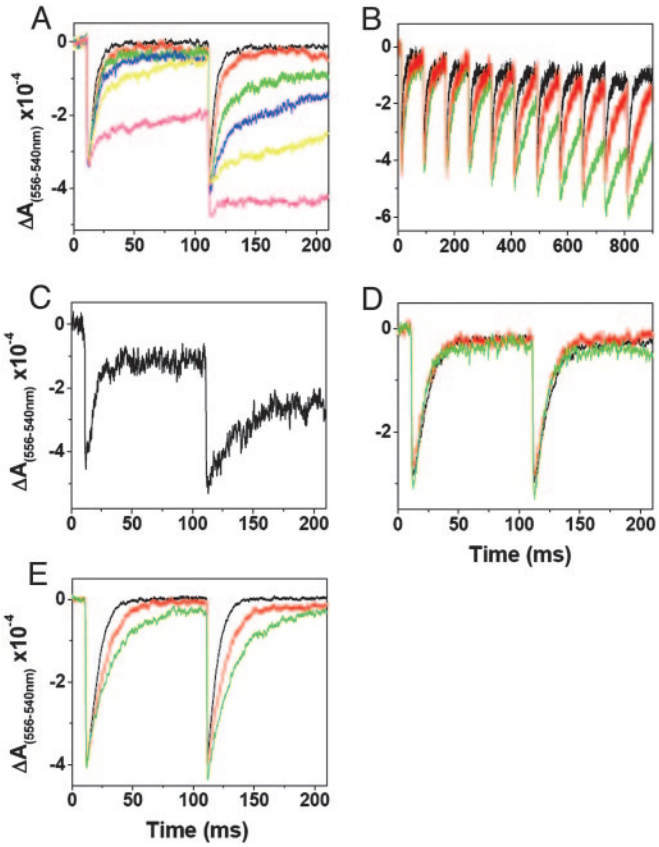

Fig. 4. Effect of DBMIB on the multiple flash-induced oxidation and reduction of cytochrome f/c_6 in *Synechococcus* sp. PCC 7002 (cells suspended at 5 μM chlorophyll, *A* and *C–E*) and cytochrome *f* in spinach thylakoids (suspended at 40 μM chlorophyll with 50 μM duroquinol, *B*). (*A*) WT^S of *Synechococcus* without DBMIB (black) or with 0.1 μM DBMIB (red), 0.3 μM DBMIB (green), 0.5 μM DBMIB (blue), 0.8 μM DBMIB (yellow), or 2 μM DBMIB (magenta). (*B*) Spinach thylakoids without DBMIB (black) or with 50 nM DBMIB (red) or 100 nM DBMIB (green). (*C*) WT^S of *Synechococcus* with 0.75 μM DBMIB under oxidizing conditions poised by the addition of 5 μM benzoquinone. (*D* and *E*) Mutants of ISP-L111A (*D*) and ISP-L111Y (*E*) of *Synechococcus*, without DBMIB (black) or with 2 μM DBMIB (red) or 50 μM DBMIB (green). The interval between two successive flashes is 100 ms for all measurements in *A* and *C–E* and 80 ms for *B*.

b_6f complex was measured in intact cells of the closely related and genetically transformable cyanobacterium, *Synechococcus* sp. PCC 7002, using the rate of reduction of cytochromes *f* and c_6 after exposure to a light flash (21, 29) (Fig. 4*A*). A short saturating actinic flash triggered oxidation of photosystem I and subsequent oxidation of cytochromes *f* and c_6 in 100–200 μs. In the absence of inhibitor, oxidation was followed by a reduction in several ms ($t_{1/2}$ = 3–10 ms) of cytochromes *f* and c_6. In the presence of DBMIB, a "turnover-enhanced inhibition" of the cytochrome *f* and c_6 reduction was observed. Reduction of cytochrome f/c_6 after the first flash was relatively insensitive to DBMIB, although with high concentrations of DBMIB (>2 μM), it was almost fully inhibited (Fig. 4*A*). However, reduction of cytochrome f/c_6 after the second flash (dark time between flashes, 100 ms), was >2-fold more sensitive to DBMIB. Further increase in the flash number could only slightly enhance the inhibition (data not shown). This turnover-enhanced inhibition has not been observed with any other inhibitors, e.g., stigmatellin, TDS, dinitrophenylether of iodonitrothymol (DNP-INT), 5-*n*-heptyl/undecyl-6-hydroxy-4,7-dioxobenzothiazole (UHDBT), 2-nonyl-4-hydroxyquinoline *N*-oxide (NQNO), and methoxyacrylate (MOA)-stilbene, of the b_6f complex in *Synechococcus* sp. PCC 7002.

Similar measurements were made with spinach thylakoids. As previously observed in pea thylakoids (33), a small, but progressive, increase in the inhibition of the cytochrome *f* re-reduction by DBMIB could be observed under multiple flash conditions in the presence of 50 or 100 nM DBMIB (≈0.6 or 1.2 DBMIB per monomer), which gave 73% or 92% inhibition in the rate of cytochrome *f* reduction after 11 flash-induced turnovers of the complex (Fig. 4*B*). The requirement of multiple flashes to elicit inhibition by DBMIB implies a relatively inefficient reaction, presumably because DBMIB was reduced to the noninhibitory form, $DBMIBH_2$, by exogenously added duroquinol (≥50 μM) (33). A more efficient light-activated inhibition by DBMIB was seen in intact *Synechococcus* cells, in the absence of added reductant, at any of the DBMIB concentrations that were used (Fig. 4*A*). A similar result was obtained under oxidizing conditions in the presence of an excess (7-fold) of benzoquinone (5 μM, E_m = +0.28 V), through which the DBMIB (0.75 μM, E_m = +0.18 V), added at a low concentration, was kept oxidized (Fig. 4*C*). Under these oxidizing conditions, the light-activated inhibition by DBMIB cannot result from photo oxidation of reduced DBMIB, as previously proposed to explain the flash-dependent inhibition obtained in the presence of DBMIB and an excess of duroquinol (33).

The DBMIB Binding Site Close to the [2Fe-2S] Cluster Is Responsible for Inhibition. Mutation of the conserved ISP residue Leu-111 (Fig. 2) of the ISP, which is involved in the formation of the Q_p site in both b_6f and bc_1 complexes (21, 34, 35), to Ala or Tyr led to a complete or an almost complete loss of sensitivity, on both first and second flashes, of the b_6f complex to DBMIB (Fig. 4 *D* and *E*). Thus, both the "dark" and "light-activated" DBMIB inhibition must be associated with an inhibitor binding site that is close to the [2Fe-2S] cluster and perturbs its EPR spectrum (Fig. 3 and refs. 25, 26, 32, and 36). This site is a lower-affinity site for binding of oxidized DBMIB, as it was not associated with significant density in the electron density map.

Discussion

Light-Induced Transfer of the Tightly Bound DBMIB Molecule: A Hypothesis. The peripheral high-affinity binding site of the oxidized quinone analogue inhibitor, DBMIB, defined by x-ray structure analysis (Figs. 1 and 2) to be 19 Å from the iron-sulfur cluster, seems anomalous in terms of a possible function as an inhibitor. DBMIB is well outside the domain occupied by the set of distally located quinone analogue inhibitors found in structure analysis of the bc_1 complex (Fig. 6). DBMIB bound at this peripheral site does not interact with the [2Fe-2S] cluster (Fig. 3), and the site is not inhibitory (Fig. 4 *D* and *E*). The question is whether the peripheral site is a dead end for DBMIB binding or whether DBMIB can be transferred in the light to an inhibitory site close to the ISP [2Fe-2S]. The present data argue for the latter. After the first flash-induced turnover of the complex, the oxidized form of DBMIB initially bound at its peripheral high-affinity site could undergo a guided diffusion to a site near the [2Fe-2S] cluster where it would exert its inhibitory effect for the second flash-induced turnover. The data supporting this inference are: (*i*) the x-ray structure shows only one DBMIB binding site, the peripheral site; (*ii*) one molecule/monomer added to the spinach (26) or *M. laminosus* (Fig. 3) b_6f complex did not perturb the g_y EPR signal of the [2Fe-2S] cluster; (*iii*) one molecule of DBMIB/monomer can inhibit electron transfer, but only after activation by light (Fig. 4*B* and refs. 24 and 33); and (*iv*) the light-activated inhibition is more efficient in the absence of exogenous reductant or under oxidizing condition (Fig. 4 *A* and *C* vs. *B*).

The movement of the DBMIB inhibitor through the complex is of interest because the pathway and mechanism by which

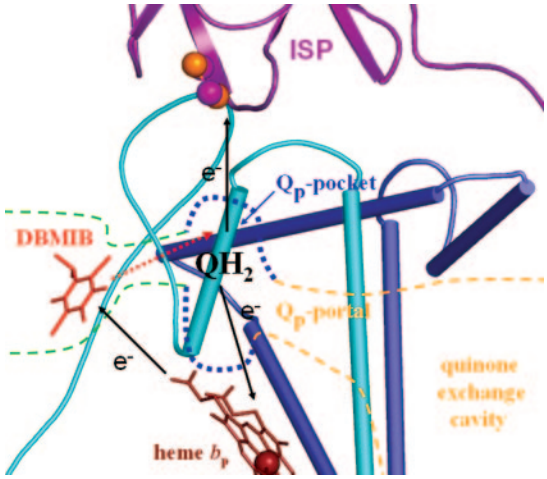

Fig. 5. Schematic diagram of the DBMIB-transfer model. The black arrows show the direction of the electron transfer, and the red dashed arrow shows the direction for the movement of DBMIB (red sticks) to the Q_p pocket. Green dotted lines indicate the peripheral DBMIB binding site and the proposed channel to the Q_p pocket.

quinone analogue inhibitors are translocated across b_6f or bc_1 complexes is not understood. This problem is made clear by the steric barrier involved in the passage of a long chain (45–50 C) PQ or ubiquinone from the intermonomer lipid-filled exchange cavity through the small 11 × 12-Å portal into the Q_p pocket and the guided diffusion of quinone analogue inhibitors into the quinone binding pocket (2, 21).

It was previously proposed that DBMIB may act like a class II inhibitor (e.g., myxothiazol) and bind at a site within the Q_p pocket, which is proximal to the heme b_p and accessible to DBMIB only after a catalytic cycle of the complex, when PQ is released (37). This model does not apply to the present case for DBMIB, because interaction with the ISP [2Fe-2S] cluster binding region is required for the inhibitory effect of the DBMIB (Fig. 4 *D* and *E*). As shown in the bc_1 complex, the ISP is not required for the binding of a class II type inhibitor, myxothiazol (38). An alternative interpretation of the light-induced progressive increase in inhibition by DBMIB in chloroplasts of higher plants, when obtained in the presence of an excess of duroquinol, which would reduce DBMIB, is that the effect of light is to oxidize noninhibitory $DBMIBH_2$ to a semiquinone or oxidized form that can bind and inhibit (33). We do not argue against occurrence of the latter mechanism for light-induced inhibition by DBMIB. However, the simplest interpretation of the appearance of inhibition after the second flash obtained with intact cells of *Synechococcus* (either no reductant added or under oxidizing conditions) (Fig. 4 *A* and *C*) is that inhibition results from light-driven movement of DBMIB from its peripheral site presumably after photo reduction to a semiquinone to the [2Fe-2S] cluster.

The peripheral DBMIB binding site seen in the *M. laminosus* structure is close to heme b_p (edge to edge, ≈8 Å) (Figs. 2 and 5). Thus, rapid electron transfer ($t_{1/2} < 1$ μs) from heme b_p ($E_{m7} = -50$ to -150 mV) (39, 40) to the DBMIB [E_{m7}(DBMIB/DBMIB$^{\cdot-}$)] = +70 mV] (41) bound at this peripheral site (Fig. 5) is feasible (42, 43). This electron transfer may account for the observation that the amplitude of the flash-induced cytochrome b_6 reduction and the slow electrochromic phase were decreased by DBMIB in spinach thylakoids (31) and *C. reinhardtii* (37). It was suggested from EPR studies that the semiquinone form of DBMIB was stabilized at the Q_p site by formation of a complex with the reduced [2Fe-2S] cluster (25, 36), and its binding affinity was significantly higher than that of the fully oxidized form in the spinach b_6f complex (25). It is proposed here that reduction of DBMIB to the semiquinone form by heme b_p leads to a switch of the higher-affinity site for DBMIB binding from the peripheral site to the Q_p pocket, where it can form a hydrogen bond with the His-129 ligand of the [2Fe-2S] cluster. The dissociation of DBMIB from the peripheral binding site might also be facilitated by electrostatic repulsion between the negatively charged DBMIB semiquinone and the overall negative binding environment that arises from the acidic residues, Asp-141 of cytochrome b_6, Glu-64 and Glu-74 of subunit IV, and Asp-243, Asp-244, and Glu-246 of cytochrome *f* that surround this site.

Based on the above considerations, a DBMIB semiquinone transfer model (Fig. 5) is proposed to explain the turnover-enhanced inhibition (Fig. 4 *A–C*). In dark-adapted cells, DBMIB binds preferentially at the peripheral noninhibitory site. During the first turnover of the complex, electron transfer is only slightly inhibited when the amount of DBMIB is insufficient for significant binding at the [2Fe-2S] site, and the DBMIB semiquinone is generated at the peripheral binding site through reduction by heme b_p. The DBMIB semiquinone has a higher binding affinity at the reduced [2Fe-2S] cluster in the Q_p pocket, which leads to transfer of the DBMIB semiquinone through a channel to the Q_p pocket where it inhibits further turnover of the complex. A possible channel that connects the peripheral DBMIB binding niche to the Q_p pocket is identified in the structure (Fig. 1*B*). This channel is formed by residues 142–144 (QVG) and 146(W) at the N-terminal part of the small *cd*1 helix in cytochrome b_6 and residues 72–76 (PLEIL) of the *ef* loop in subunit IV (Fig. 2).

Pathway of Transfer Across the Membrane. DBMIB is a smaller and less hydrophobic molecule than PQ and other *p*-side quinone analogue inhibitors. The peripheral DBMIB site and the channel to the Q_p pocket can form an alternative pathway for the transport of DBMIB from membrane lipid to the Q_p pocket (Figs. 1*B* and 5). The observed DBMIB molecule bound at the peripheral binding site then shows the inhibitor trapped during its movement to the Q_p pocket. This pathway may not be used by the larger, more hydrophobic PQ molecule. It is, nevertheless, important to understand the passage of DBMIB through the core of the complex, because DBMIB is a frequently used *p*-side inhibitor, and to understand the movement of nonpolar molecules through the complicated, labyrinthine internal space of an integral membrane protein complex. Together with the binding site of PQ on the *n*-side of the complex (2), and ring-in, ring-out orientations of TDS seen in the structures from *C. reinhardtii* (3) and *M. laminosus* (2, 21), the peripheral high-affinity binding site of DBMIB contributes to a total of four potential sites for quinone/quinol binding that provide markers for their transfer through the b_6f complex.

We thank H. Zhang for helpful discussions. This study was supported by National Institutes of Health Grant GM-38323 (to W.A.C.) and a Fellowship from the Japanese Ministry of Science and Education (to G.K.). The x-ray structure analysis, on which this study is based, was carried out on beamline SBC-19ID at the Advanced Photon Source, Argonne National Laboratory, Argonne, IL, which is supported by U.S. Department of Energy Grant W31-109-ENG-389, and at Spring-8 BL44XU (Hyogo, Japan).

1. Blankenship, R. E. (2002) *Molecular Mechanisms of Photosynthesis* (Blackwell, Malden, MA), pp. 124–156.
2. Kurisu, G., Zhang, H., Smith, J. L. & Cramer, W. A. (2003) *Science* **302,** 1009–1014.
3. Stroebel, D., Choquet, Y., Popot, J. L. & Picot, D. (2003) *Nature* **426,** 413–418.
4. Xia, D., Yu, C. A., Kim, H., Xia, J. Z., Kachurin, A. M., Zhang, L., Yu, L. & Deisenhofer, J. (1997) *Science* **277,** 60–66.
5. Zhang, Z., Huang, L., Shulmeister, V. M., Chi, Y. I., Kim, K. K., Hung, L. W., Crofts, A. R., Berry, E. A. & Kim, S. H. (1998) *Nature* **392,** 677–684.
6. Kim, H., Xia, D., Yu, C. A., Xia, J. Z., Kachurin, A. M., Zhang, L., Yu, L. & Deisenhofer, J. (1998) *Proc. Natl. Acad. Sci. USA* **95,** 8026–8033.
7. Hunte, C., Koepke, J., Lange, C., Rossmanith, T. & Michel, H. (2000) *Structure (London)* **8,** 669–684.

8. Gao, X., Wen, X., Yu, C., Esser, L., Tsao, S., Quinn, B., Zhang, L., Yu, L. & Xia, D. (2002) *Biochemistry* **41,** 11692–11702.
9. Gao, X., Wen, X., Esser, L., Quinn, B., Yu, L., Yu, C. A. & Xia, D. (2003) *Biochemistry* **42,** 9067–9080.
10. Palsdottir, H., Lojero, C. G., Trumpower, B. L. & Hunte, C. (2003) *J. Biol. Chem.* **278,** 31303–31311.
11. Esser, L., Quinn, B., Li, Y. F., Zhang, M., Elberry, M., Yu, L., Yu, C. A. & Xia, D. (2004) *J. Mol. Biol.* **341,** 281–302.
12. Widger, W. R., Cramer, W. A., Herrmann, R. G. & Trebst, A. (1984) *Proc. Natl. Acad. Sci. USA* **81,** 674–678.
13. Smith, J. L., Zhang, H., Yan, J., Kurisu, G. & Cramer, W. A. (2004) *Curr. Opin. Struct. Biol.* **14,** 432–439.
14. Berry, E. A., Guergova-Kuras, M., Huang, L. S. & Crofts, A. R. (2000) *Annu. Rev. Biochem.* **69,** 1005–1075.
15. Cramer, W. A., Zhang, H., Yan, J., Kurisu, G. & Smith, J. L. (2004) *Biochemistry* **43,** 5921–5929.
16. Joliot, P. & Joliot, A. (1986) *Biochim. Biophys. Acta* **849,** 211–222.
17. Joliot, P. & Joliot, A. (1994) *Proc. Natl. Acad. Sci. USA* **91,** 1034–1038.
18. Kallas, T. (1994) in *The Molecular Biology of Cyanobacteria*, ed. Bryant, D. A. (Kluwer, Dordrecht, The Netherlands), pp. 259–317.
19. Crofts, A. R., Shinkarev, V. P., Kolling, D. R. & Hong, S. (2003) *J. Biol. Chem.* **278,** 36191–36201.
20. Crofts, A. R. (2004) *Annu. Rev. Physiol.* **66,** 689–733.
21. Yan, J. & Cramer, W. A. (2004) *J. Mol. Biol.* **344,** 481–493.
22. Trebst, A., Harth, E. & Draber, W. (1970) *Z. Naturforsch. B* **25,** 1157–1159.
23. Malkin, R. (1986) *FEBS Lett.* **208,** 317–320.
24. Graan, T. & Ort, D. R. (1986) *Arch. Biochem. Biophys.* **248,** 445–451.
25. Schoepp, B., Brugna, M., Riedel, A., Nitschke, W. & Kramer, D. M. (1999) *FEBS Lett.* **450,** 245–250.
26. Roberts, A. G. & Kramer, D. M. (2001) *Biochemistry* **40,** 13407–13412.
27. Zhang, H., Kurisu, G., Smith, J. L. & Cramer, W. A. (2003) *Proc. Natl. Acad. Sci. USA* **100,** 5160–5163.
28. Buzby, J. S., Porter, R. D. & Stevens, S. E., Jr. (1985) *Science* **230,** 805–807.
29. Yan, J. & Cramer, W. A. (2003) *J. Biol. Chem.* **278,** 20925–20933.
30. Ponamarev, M. V. & Cramer, W. A. (1998) *Biochemistry* **37,** 17199–17208.
31. Robert, W. J. & Whitmarsh, J. (1988) *Biochim. Biophys. Acta* **933,** 258–268.
32. Roberts, A. G., Bowman, M. K. & Kramer, D. M. (2004) *Biochemistry* **43,** 7707–7716.
33. Rich, P. R., Madgwick, S. A. & Moss, D. A. (1991) *Biochim. Biophys. Acta* **1058,** 312–328.
34. Liebl, U., Sled, V., Brasseur, G., Ohnishi, T. & Daldal, F. (1997) *Biochemistry* **36,** 11675–11684.
35. Brasseur, G., Sled, V., Liebl, U., Ohnishi, T. & Daldal, F. (1997) *Biochemistry* **36,** 11685–11696.
36. Malkin, R. (1981) *FEBS Lett.* **131,** 169–172.
37. Barbagallo, R. P., Finazzi, G. & Forti, G. (1999) *Biochemistry* **38,** 12814–12821.
38. Brandt, U., Haase, U., Schagger, H. & von Jagow, G. (1991) *J. Biol. Chem.* **266,** 19958–19964.
39. Kramer, D. M. & Crofts, A. R. (1994) *Biochim. Biophys. Acta* **1184,** 193–201.
40. Girvin, M. E. & Cramer, W. A. (1984) *Biochim. Biophys. Acta* **767,** 29–38.
41. Rich, P. R. & Bendall, D. S. (1980) *Biochim. Biophys. Acta* **592,** 506–518.
42. Page, C. C., Moser, C. C. & Dutton, P. L. (2003) *Curr. Opin. Chem. Biol.* **7,** 551–556.
43. Gray, H. B. & Winkler, J. R. (2005) *Proc. Natl. Acad. Sci. USA* **102,** 3534–3539.